Volume 14, Issue 2, 142414 (1-10)

Iranian Journal of Catalysis (IJC)

https://doi.org/10.57647/j.ijc.2024.1402.14

Electronic band gap calculation of N, Co, and (N, Co) single- and dual-doped rutile phase: a hybrid periodic DFT study

Reza Behjatmanesh-Ardakani[1]*, Ahlam Moradzadeh[2], Tamerlan T. Magkoev[3]

[1]*Department of Chemical Engineering, Faculty of Engineering, Ardakan University, Ardakan, Iran.*
[2]*Department of Chemistry, Payame Noor University, Tehran, Iran.*
[3]*Laboratory of Adsorption Phenomena, Department of Condensed Matter Physics, North Ossetian State University, Vatutina, Vladikavkaz, Russia.*

*__Corresponding authors:__ behjatmanesh@ardakan.ac.ir; reza_b_m_a@yahoo.com

Review Paper

Received:
14 January 2024
Revised:
15 February 2024
Accepted:
3 April 2024
Published online:
1 June 2024

Abstract:

TiO_2 is a highly desirable photocatalyst due to its abundance and low cost. However, its large band gap restricts its ability to absorb a significant portion of visible light. This issue can be addressed through cationic or anionic doping. In these instances, the impurity bands reduce the band gap. Nevertheless, in order to enhance the photocatalytic activity, these bands need to be distributed among the atoms. In this study, we investigated the electronic structures of rutile bulk phases co-doped with cobalt and nitrogen. Data show that the single doping of rutile by N and Co reduces the band gap by 26% and 42%, respectively. For the (N, Co) dual-doped rutile, the band gap value depends on the relative position of the dopants. When placed in the nearest neighbor configuration (*nearest* model), the band gap only decreases by 25%. However, if the dopants are positioned far from each other (*far* model), the catalyst becomes half-metallic with the spin-down channel's band gap equal to zero. The calculated spatial delocalization indices (*SDI*) for the impurity bands reveal that the *far* model of (N, Co) dual-doped TiO_2 exhibits the highest *SDI* value compared to the other cases. All studied catalysts displayed magnetic properties. The magnetic moments of single-doped catalysts are 1 μB, while the magnetic moment of the dual-doped catalyst is 2 μB.

Keywords: Co-doped; Dual-doped; N-doped; Rutile; TiO_2

1. Introduction

Rutile and anatase are used in various industries, including solar cells, gas sensors, and catalysis for pollutant degradation. However, their large band gaps restrict their absorption of ultraviolet radiation, which accounts for only 5% of the solar spectrum [1]. The rutile phase also suffers from electron-hole recombination, reducing its photocatalytic activity. To address this issue, new bands can be introduced in the forbidden region through elemental substitutional doping [2–5], a technique widely employed in recent researches to reduce the band gap [6, 7].

Nitrogen is the most common non-metal dopant (see, for example, [8] and its references). However, there are contradictory data regarding the photocatalytic activity of N-doped TiO_2. On one hand, Asahi et al. reported a narrowed band gap of N-doped TiO_2 by mixing O 2p orbitals with N 2p orbitals [9], while on the other hand, Lindgren et al. showed that only some localized N 2p orbitals formed on the top of VBM, resulting in no obvious gap reduction [10]. Modeling data indicate that not only the concentration of nitrogen atoms but also the relative position of two dopants affects the band gap narrowing [11]. Doping with metals can also be utilized to manipulate the band gap of both

rutile and anatase. This is achieved by placing the *d* orbitals of the dopant below the conduction band minimum (CBM), leading to a reduction of the band gap (see, for example, [12, 13]). There are numerous other examples where transition metal dopants have been shown to enhance the photocatalytic activity of TiO_2. However, single dopants decrease the band gap by a small value, which is insufficient for photocatalytic activities in the visible light range [14]. To address this issue, dual-doping (or co-doping) has been used in literature to further narrow the band gap. These dopants can be either all cations or a mixture of anions and cations (see, for example, [15–17]).

The reduction of the band gap due to the presence of impurities does not always increase the photocatalytic properties. If the impurity bands are localized, they act as recombination centers, and reducing the band gap does not lead to an increase in the photocatalytic properties [9]. It is necessary to ensure that there is sufficient overlap of dopant bands with TiO_2 band states in order to bring the generated carriers to the catalyst surface within their lifetime. Therefore, it is important to check the density of impurity eigenstates to determine if they are localized or distributed on different atoms in the lattice. Kuo et al. utilized a participation ratio (*pi*) to quantify the delocalization of the wave-functions of these impurity bands [11]. Bands with a *pi* value of unity are highly delocalized, while smaller *pi* values indicate that only a certain part of the cell contributes to the electronic eigenstate. If the impurity bands have a much smaller value of *pi* compared to the VBM and CBM, they act as recombination centers. In this case, the band gap is reduced, but the photocatalytic activity is not increased. Quantifying the delocalization of dopant bands can help in predicting the photocatalytic activity of proposed compounds.

In this paper, we employed a different method to quantify the delocalization of the impurity bands by calculating electronic densities. This method, based on the spatial delocalization index (*SDI*), measures the degree of delocalization of impurity bands. We selected cobalt/nitrogen dual dopants for band gap engineering of the TiO_2 rutile phase, as both single Co doping [18–24] and Co/N dual doping [19–25] have been widely studied experimentally for band gap reduction. Conversely, there are few theoretical studies in the literature on Co-doped TiO_2 (see, for example, [26, 27]), and there are no theoretical studies on Co/N dual-doped rutile phase. None of these theoretical studies have discussed the role of their impurity bands as recombination centers of electron-hole pairs or as active centers that can enhance photocatalytic activity. In this paper, we utilized the PBE0 hybrid level of theory to carefully calculate both the band gap reductions and the *SDI* of impurity levels to examine whether these impurity bands contribute to enhancing photocatalytic properties.

2. Experimental

Periodic full-potential DFT calculations were performed using the FHI-aims code to optimize the lattice parameters and atomic positions of a pure and doped $2\times2\times2$ supercell of rutile bulk phase [28–31]. Both single and dual-doped rutile cases were examined to investigate the effects of dopant bands on the band structure of rutile. In the studied cases, N (Co), replaces the O (Ti) atom. A K-grid of $3\times3\times6$, generated by the Monkhorst-Pack algorithm, was used to sample the first Brillouin zone [32]. The spin-collinear version of the self-consistence field method was employed for all cases. PBE functional [33] was utilized to optimize the crystals, and the hybrid-PBE0 (with α=0.18) was used for post-processing band structure calculations [34]. Scalar relativistic effects were accounted for in all calculations using Zero Order Regular Approximation (ZORA). The SCF convergence criteria for energy and density were set to be less than 10^{-5} and 10^{-4} eV, respectively, with structures fully optimized until the force was less than 0.05 eV/Å. The spatial delocalization index (*SDI*) for all impurity bands, as well as valence and conduction bands, was calculated according to the formula defined by Lu [35]:

$$SDI = \frac{1}{\sqrt{\int |f_{norm}(\underline{r})|^n d\underline{r}}}, \qquad f_{norm}(\underline{r}) = \frac{f(\underline{r})}{\int f(\underline{r}) d\underline{r}} \tag{1}$$

In the standard definition of *SDI*, the value of *n* is equal to 2, where f_{norm} is a normalized function. It is convenient to utilize the following equation for calculating the *SDI* of a band *i*:

$$SDI_i = \frac{1}{\sqrt{\int |\rho_i(\underline{r})|^2 d\underline{r}}}, \qquad \rho_i(\underline{r}) = |\varphi_i(\underline{r})|^2 \tag{2}$$

The Multiwfn program [35] was employed to compute the *SDI* for the selected bands in order to assess their distribution in three-dimensional space. Additionally, their electron densities were visualized using the VESTA code [36].

3. Results and Discussion

3.1 Model Verification

The optimization of the rutile bulk phase using the employed model revealed that the calculated unit cell lattice parameters are *a*=*b*=4.69, *c*=2.99, α=90, β=90, and γ=90 with only a +2% deviation from the experimental data. The axial Ti-O bond length measures 1.97 Å, while the equatorial bond length is 2.03 Å, representing a +1% and +2.5% difference from the experimental data, respectively. The theoretical band gap is determined to be 3.05 eV, showing a +2% deviation from the experimental value of 3.0 eV. Notably, the band gap is direct, from the gamma point in the valence band to the gamma point in the conduction band (see Fig. 1 for the band structure, and Fig. 2 for the electron density and SDI for valence and conduction bands). These findings suggest that the method utilized in this study is dependable, with errors of less than 3% (in contrast to the 36% error in the model by Jha et al. [37], and the 37% error in the model by Yang [38]).

3.2 Single-doped rutile

Many theoretical (see, for example, [38–41]) and experimental methods (see, for example, [42–46]) have been used to study nitrogen-doped rutile phase. Here, we summarize our DFT data on the single N-doped rutile. Fig. 3 depicts the density of states (DOS) and band structure of the N-doped rutile phase calculated using the hybrid method. Similar to

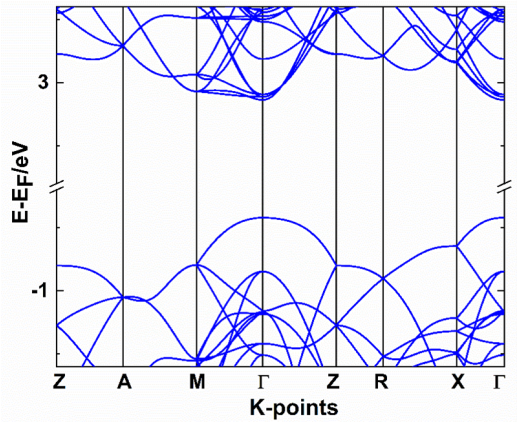

Figure 1. Band structure of the pure perfect rutile phase. The pristine rutile phase is a non-magnetic compound with identical spin-up and spin-down band energies. The gap is equal to 3.05 eV which is only 2% greater than the experimental value of 3.0 eV. The Fermi level is at -9.19 eV.

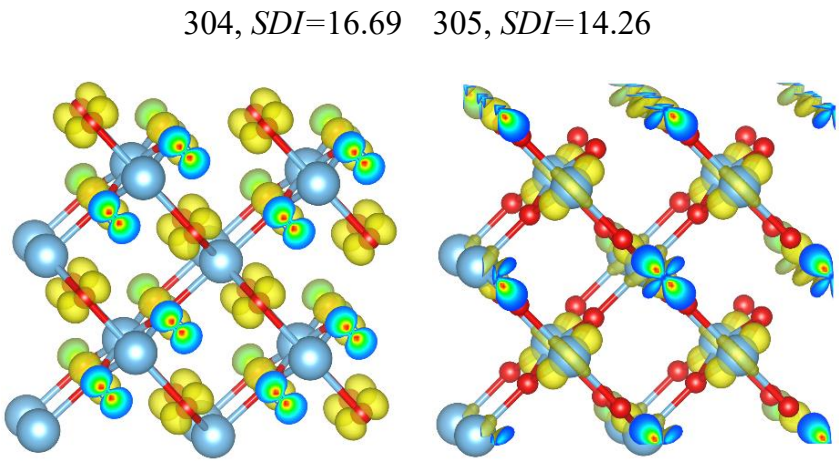

Figure 2. Electron density for valence (band number 304) and conduction (band number 305) bands of the pristine rutile phase. The iso-surface was set to 0.01 e$\AA^{-3}$. High values of *SDI* indicate that the bands are distributed throughout the entire cell, and do not serve as electron-hole recombination centers.

other DFT studies, a nitrogen defect band is localized in the band gap region, while others are in the valence band and have been hybridized with oxygen bands (see Fig. 4 for the electron density and SDI of the valence and conduction bands).. Our data indicates that N-doping shifts the Fermi level up by 0.1 eV, and that hybrid total magnetic moment of N-doped rutile equals $1\mu_B$, consistent with the experimental value of 0.9 [47] and theoretical data [41–48] in this field. The band gap for the spin-up channel (3.25 eV) is 7% higher than that of pure rutile, while the band gap for the spin-down channel (2.25 eV) is 26% less than that of pure rutile. Consequently, the minority spin channel can absorb visible light from sunlight and increase rutile's efficiency as a photocatalyst (the data is consistent with the other studies, for example [38, 48–51]).

The other single dopant which we studied is cobalt. Cobalt is a transition metal that has been widely used in experimental works for doping TiO_2. For example, Ferreira et al. employed the hydrothermal method to synthesize Co-doped TiO_2 for the degradation of triclosan [19]. They reported a single band gap of 2.8 eV for their Co-doped TiO_2, while their Tauc plot exhibited two linear regions. The Kubelka-Munk model [52, 53], which forms the basis of the Tauc plot, can be considered for both spin-up (α) and spin-down (β) as follows:

$$(\varepsilon h\nu)^p \propto [(E - E_g^{spin-up}) + (E - E_g^{spin-down})] \qquad (3)$$

where ε is the absorption coefficient, p is a constant that determines type of transition (p=2 for direct allowed transition, p=1/2 for indirect allowed transition), E stands for incident photon energy, $E_g^{spin-up}$ denotes the spin-up band gap, and $E_g^{\beta spin-down}$ represents the spin-down band gap.

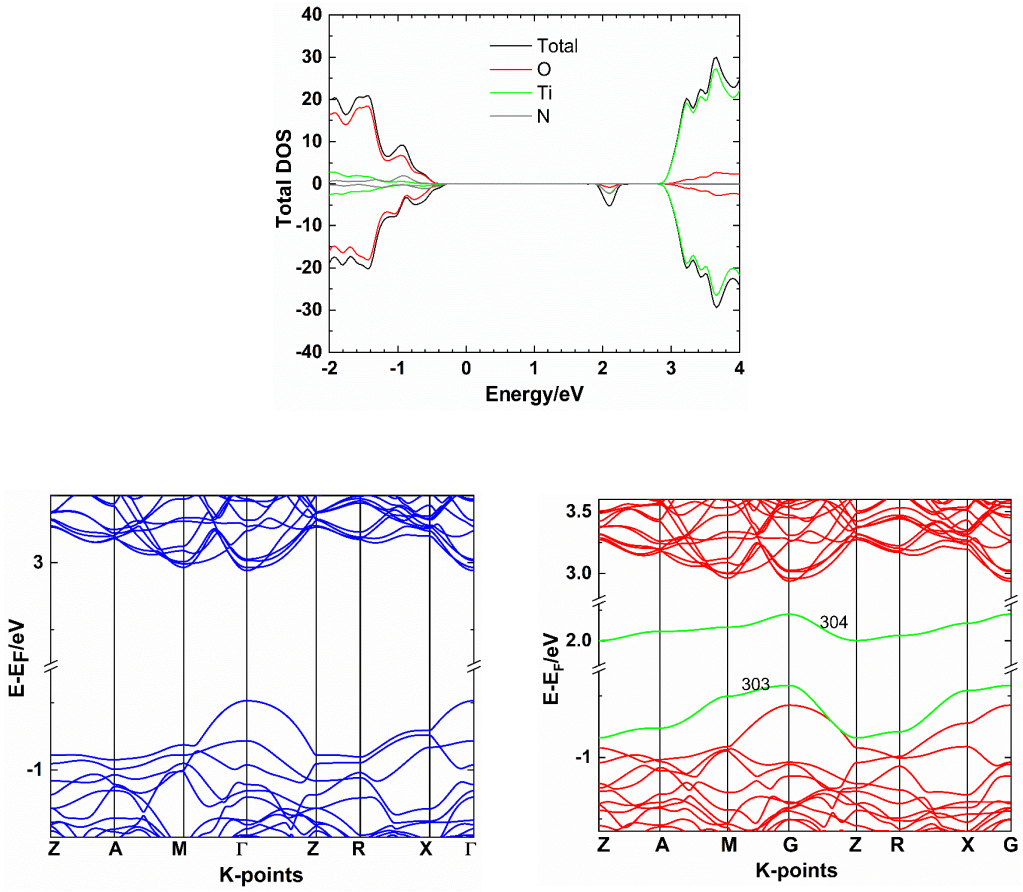

Figure 3. DOS (up) and band structures (down) of the N-doped rutile phase for the spin-up and spin-down channels. The spin-up and spin-down gaps are 3.25 and 2.25 eV, respectively. The Fermi level is at -9.08 eV. The spin-up gap increased by 7%, while the spin-down gap decreased by 26% compared to the pure rutile. The band structure for the spin-up channel is depicted in blue, and the band structure for spin-down channel is depicted in red. The green lines represent the impurity bands, with band number 303 being occupied and band number 304 being empty.

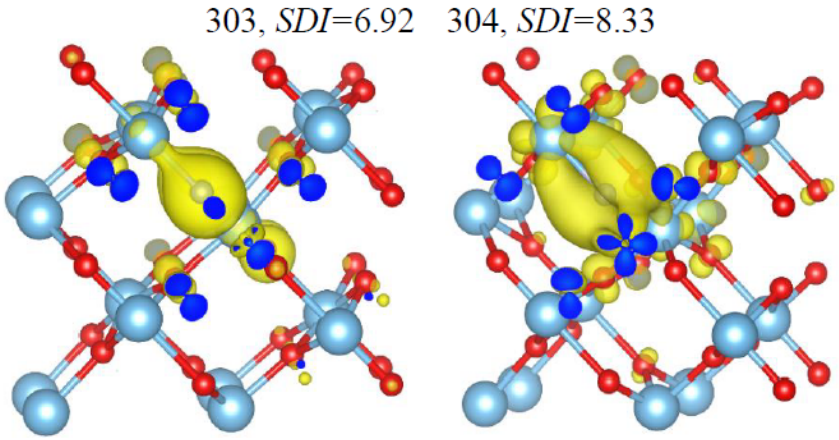

Figure 4. Electron density for two impurity bands in the spin-down channel (303 and 304) of the N-doped rutile phase. The iso-surface was set to 0.01 e$\AA^{-3}$. The sum of the *SDI* for all impurity bands in the spin-down channel is 15.25.

Consequently, the presence of two straight lines in the Tauc plot can be attributed to two band gaps, one for spin-up, and the other for spin-down channels. A detailed examination of the Tauc plot in Ferreira et al.'s work reveals two broken lines with distinct slopes, indicating the presence of two different band gaps. The first line had a lower slope value and intersected the x-axis at approximately 1.7 eV, while the other line intersected it at around 1.6 eV (refer to Fig. 2b in [19]). Fig. 6 shows the electron density and SDI of impurity bands in Co-doped rutile phase. Our calculated hybrid data (see Fig. 5) shows two band gaps (1.78 eV for spin-up and 1.80 eV for spin-down electrons), which are consistent with the band gaps observed in experiments. The magnetic moment of Co-doped rutile is 1 μ_B. Similar to Ti, Co is in a +4-oxidation state and possesses one unpaired electron in t_{2g}. The substitutional doping of Co alters the Fermi level of rutile from -9.2 eV to -8.1 eV. Since the valence band is primarily composed of orbitals centered on oxygen atoms, the shift in the Fermi level indicates a reduction in the electrostatic interaction between protons and electrons in oxygen atoms. This decrease is attributed to a reduction in the charge density of oxygen atoms. The calculation of Hirshfeld charge reveals that Co possesses 60% of the charge of the Ti atom, while the charges on oxygen atoms have been decreased compared to those in the pure rutile phase.

3.3 Dual-doped rutile

Two models were constructed for (N, Co) dual-doped rutile. In the first mode (*nearest* model), Co and N dopant atoms are positioned as nearest neighbors, while in the other model (*far* model), their positions are more distant from each other. Fig. 7 illustrates the DOS of these two models. The *nearest* model indicates band gaps of 2.8 eV and 2.25 eV for spin-up and spin-down electrons, respectively (see Fig. 8 for the electron density and SDI of the impurity bands). The *far* model shows band gaps of 2.00 eV and zero for spin-up and spin-down electrons, respectively (see Fig. 9 for the band structure, and Fig. 10 for the electron density and SDI of impurity bands). Data indicate that in the *far* mode, the dopant atoms exhibit synergistic effects. For the spin-down channel, the band gap becomes zero, suggesting that the model predicts half-metallic properties that could be advantageous for spintronics. This result is consistent with the findings of Ferreira et al. [19], who utilized the Tauc plot to determine the band gaps of single Co and (N, Co) dual-doped TiO_2.

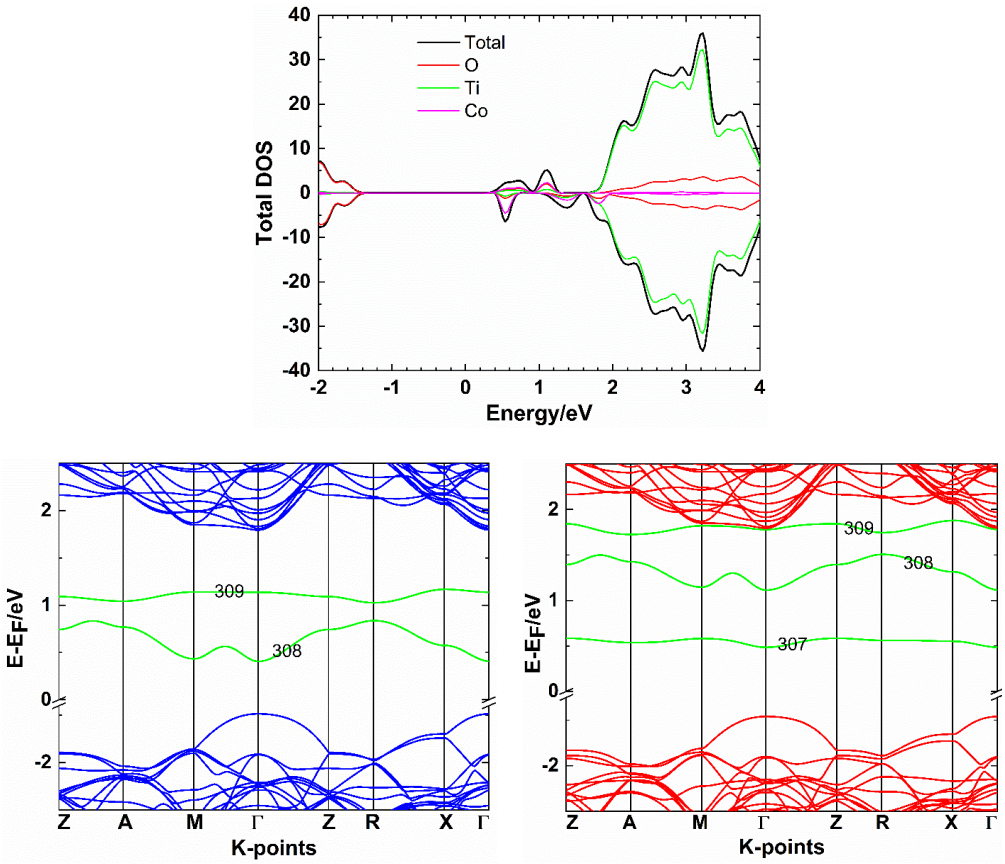

Figure 5. DOS (up) and band structures (down) of the Co-doped rutile phase for the spin-up and spin-down channels. The spin-up and spin-down gaps are 1.78 and 1.80 eV, respectively. The Fermi level is at -8.1 eV. The spin-up gap decreases by 42%, and the spin-down gap decreases by 41% compared to the pure rutile. All impurity bands (green lines) are empty.

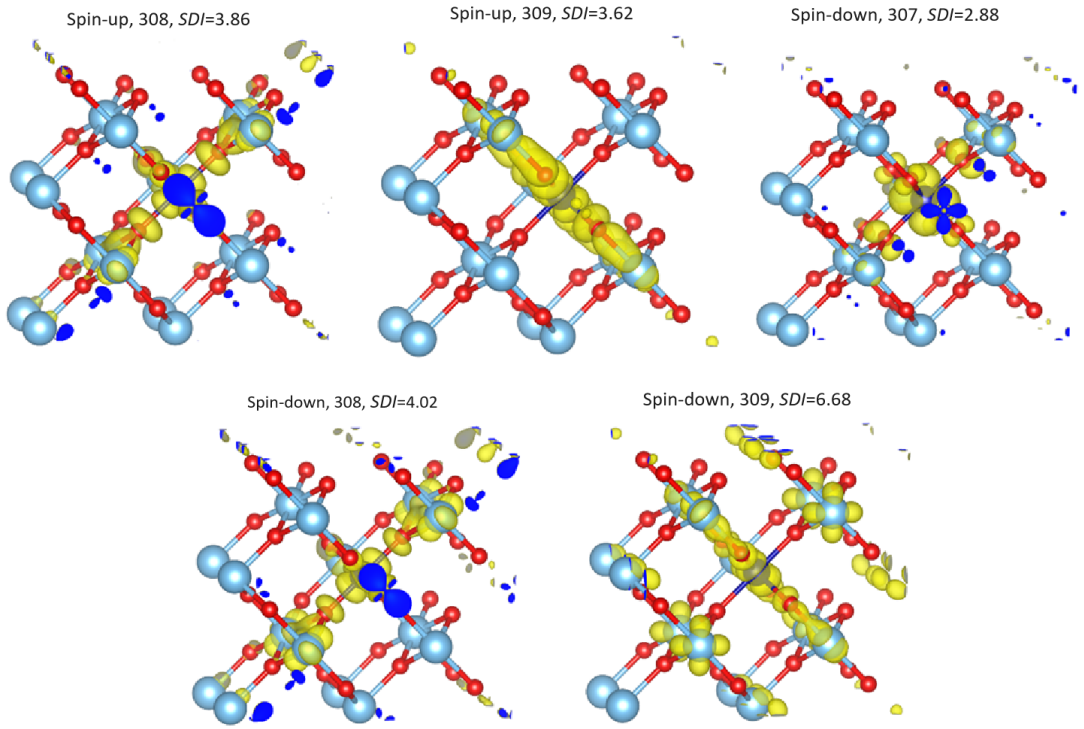

Figure 6. Electron density for two impurity bands in the spin-up channel (308 and 309) and three impurity bands in the spin-down channel (307, 308, and 309) of Co-doped rutile phase. The iso-surface was set to 0.01 e$\AA^{-3}$. The sum of the *SDI* for all impurity bands in spin-up and the spin-down channels are 7.48 and 13.58, respectively.

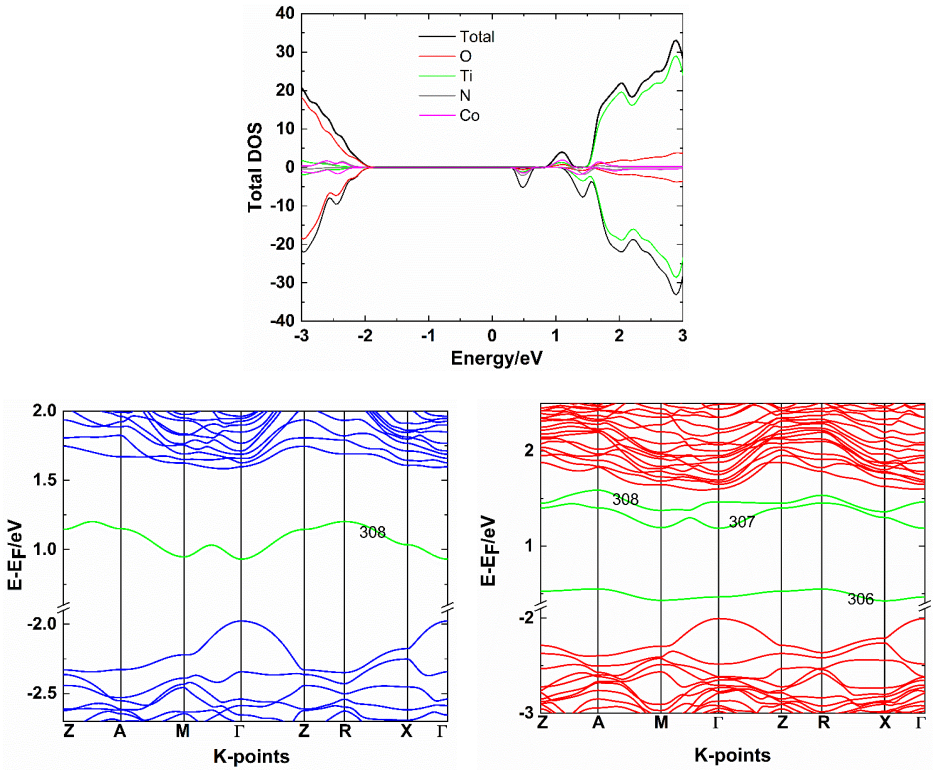

Figure 7. Total and partial DOS for the (N, Co)-doped '*nearest*' model rutile phase. The spin-up and spin-down gaps are 2.80 and 2.25 eV, respectively. The Fermi level is at -7.61 eV.

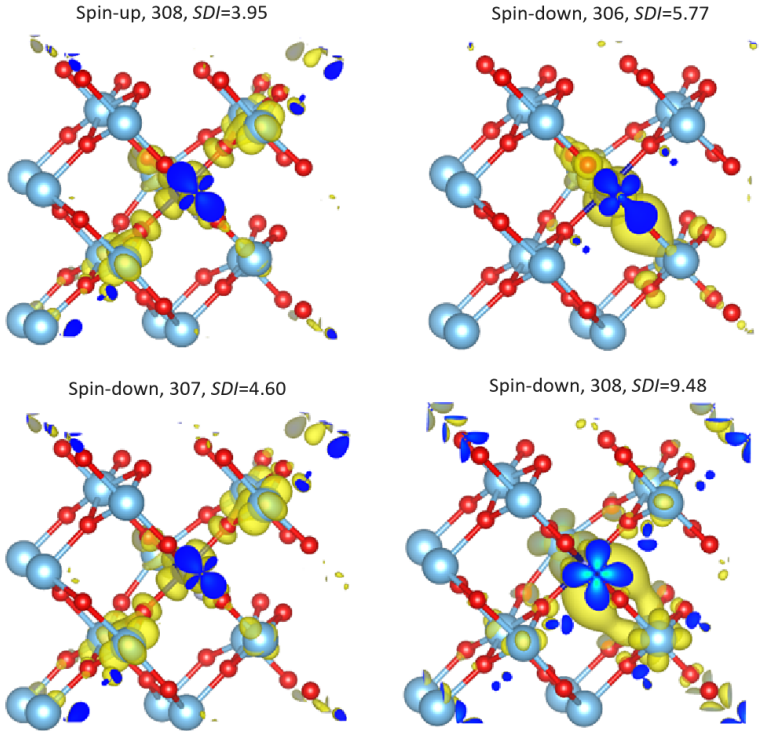

Figure 8. Electron density for one spin-up (band number 308) and three spin-down impurity bands (306-308) of the *nearest* model rutile phase. The iso-surface was set to 0.01 e$\AA^{-3}$. The sum of the *SDI* for all impurity bands in spin-up and spin-down channels are 3.95 and 19.85, respectively.

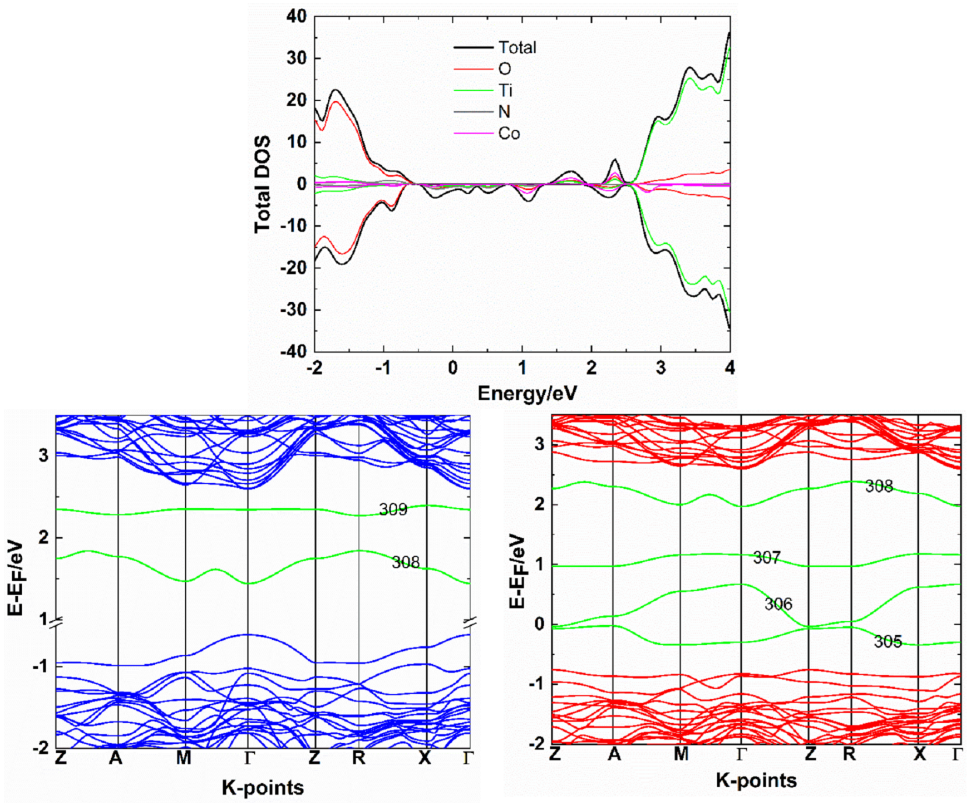

Figure 9. DOS (up) and band structures (down) of the (N, Co)-doped *far* model rutile phase. The spin-up and spin-down gaps are 2.00 and 0.00 eV, respectively. The Fermi level is at -8.9 eV.

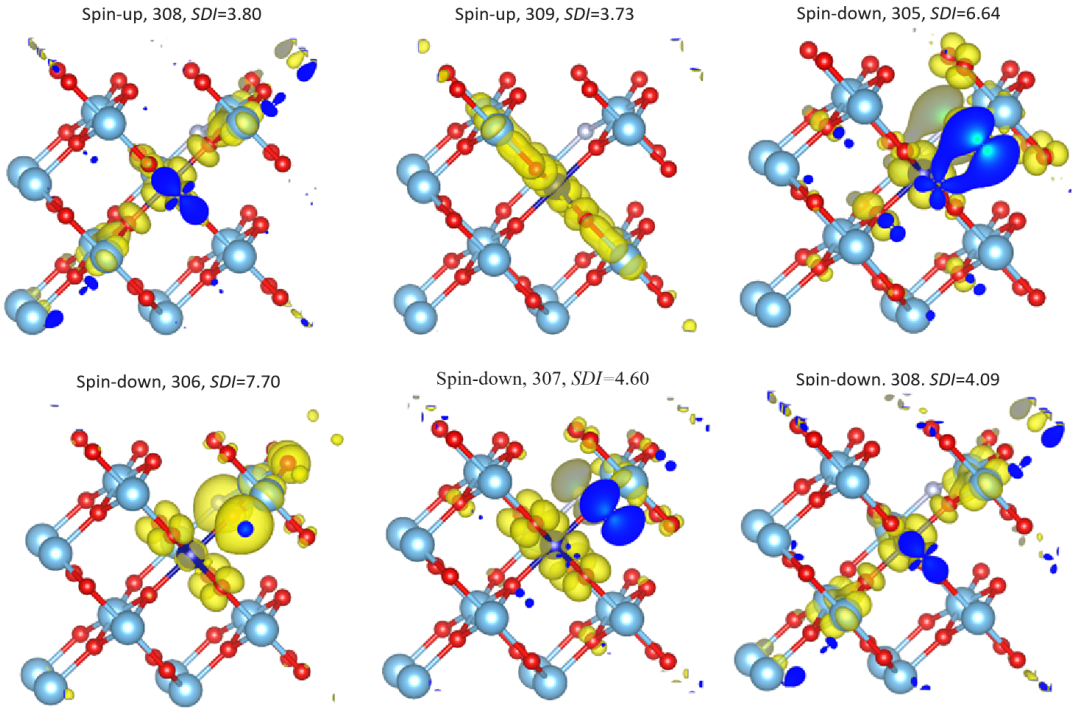

Figure 10. Electron density for two spin-up (band numbers 308−309) and four spin-down impurity bands (305−308) of the *far* model rutile phase. The iso-surface was set to 0.01 e$\mathring{A}^{-3}$. The sum of the *SDI* for all impurity bands in the spin-up and spin-down channels are 7.53 and 23.03, respectively.

4. Conclusion

The electronic structures of single and dual-doped rutile phases were analyzed using the high-level PBE0 hybrid method. The hybrid data aligned with published experimental data, indicating that all single and dual-dopants reduce the band gap; however, dual doped cases have higher *SDI* values compared to the single-doped ones. The calculated band gaps correspond well with the experimental ones obtained by intersecting fitted lines with the x-axis in the Tauc plot. Hybrid data accurately predicted that (N, Co) dual-doped TiO_2 exhibits half-metallic properties suitable for spintronics. Our findings suggest that the positions of doped N and Co are crucial in band gap engineering. The magnetic moments of rutile doped by N, Co, and (N, Co) dopants are 1μB, 1μB, and 2μB, respectively.

Acknowledgments
The authors are grateful to Payame Noor and Ardakan universities for their support. The work was partly done within the State Task (Goszadanie) of the Russian Ministry of Science and Higher Education (scientific theme code # FEFN-2024-0002).

Authors Contributions
All authors have contributed equally to prepare the paper.

Availability of Data and Materials
The data that support the findings of this study are available from the corresponding author upon reasonable request.

Conflict of Interests
The authors declare that they have no known competing financial interests or personal relationships that could have appeared to influence the work reported in this paper.

References

[1] A. Bokare, M. Pai, and A. A. Athawale. ””. **91** (2013):111–119. DOI: https://doi.org/10.1016/j.solener.2013.02.005.

[2] U. M. S. Khan, M. Al-Shahry, and W. B. Ingler. ””. *Science*, **297** (2002):2243–2245. DOI: https://doi.org/10.1126/science.1075035.

[3] M. Ni, M. K. H. Leung, D. Y. C. Leung, and K. Sumathy. *Renew. Sust. Energ. Rev.*, **11** (2007):401–425. DOI: https://doi.org/10.1016/j.rser.2005.01.009.

[4] S. M. Esfandfard, M. R. Elahifard, R. Behjatmanesh-Ardakani, and H. Kargar. *Phys. Chem. Res.*, **6** (2018):547–563. DOI: https://doi.org/10.22036/PCR.2018.128713.1481.

[5] W. Choi, A. Termin, and M. R. Hoffmann. *J. Phys. Chem.*, **98** (1994):13669–13679. DOI: https://doi.org/10.1021/j100102a038.

[6] V. Hasija, P. Singh, S. Thakur, V. H. Nguyen, Q. Van Le, T. Ahamad, S. M. Alshehri, P. Raizada, B. M. Matsagar, and K. C. W. Wu. *Chemosphere*, **320** (2023):138015. DOI: https://doi.org/10.1016/j.chemosphere.2023.138015.

[7] V. Soni Sonu, P. Singh, S. Thakur, P. Thakur, T. Ahamad, V. H. Nguyen, Q. Van Le, C. M. Hussain, and P. Raizada. *J. Environ. Chem. Eng.*, **11** (2023:110856. DOI: https://doi.org/10.1016/j.jece.2023.110856.

[8] R. Asahi, T. Morikawa, H. Irie, and T. Ohwaki. *Chem. Rev.*, **114** (2014):9824–9852, . DOI: https://doi.org/10.1021/cr5000738.

[9] R. Asahi, T. Morikawa, T. Ohwaki, K. Aoki, and Y. Taga. *Science*, **293** (2001):269–271, . DOI: https://doi.org/10.1126/science.1061051.

[10] T. Lindgren, J. M. Mwabora, E. Avendaño, J. Jonsson, A. Hoel, C. G. Granqvist, and S. E. Lindquist. *J. Phys. Chem. B*, **107** (2003):5709–5716. DOI: https://doi.org/10.1021/jp027345j.

[11] C. L. Kuo, W. G. Chen, and T. Y. Chen. *J. Appl. Phys.*, **116** (2014):093709. DOI: https://doi.org/10.1063/1.4894444.

[12] A. Kerrami, L. Mahtout, F. Bensouici, M. Bououdina, S. Rabhi, E. Sakher, and H. Belkacemi. *Mater. Res. Express.*, **6** (2019):0850f0855. DOI: https://doi.org/10.1088/2053-1591/ab2677.

[13] X. Zhu, Q. Zhou, Y. Xia, J. Wang, H. Chen, Q. Xu, J. Liu, W. Feng, and S. Chen. *J. Mater. Sci.: Mater. Electron.*, **32** (2021):21511–21524. DOI: https://doi.org/10.1007/s10854-021-06660-5.

[14] A. Dashora, N. Patel, D. C. Kothari, B. L. Ahuja, and A. Miotello. *Sol. Energy Mater. Sol. Cells*, **125** (2014):120–126. DOI: https://doi.org/10.1016/j.solmat.2014.02.032.

[15] T. Y. Li, R. J. Si, J. Sun, S. T. Wang, J. Wang, R. Ahmed, G. B. Zhu, and C. C. Wang. *Sensor. Actuat. B: Chem.*, **293** (2019):151–158. DOI: https://doi.org/10.1016/j.snb.2019.05.019.

[16] A. M. Youssef and S. M. Yakout. *Mater. Chem. Phys.*, **282** (2022):125978. DOI: https://doi.org/10.1016/j.matchemphys.2022.125978.

[17] R. Rashid, I. Shafiq, M. J. Iqbal, M. Shabir, P. Akhter, M. H. Hamayun, A. Ahmed, and M. Hussain. *J. Environ. Chem. Eng.*, **9** (2021):105480. DOI: https://doi.org/10.1016/j.jece.2021.105480.

[18] V. G. Bessergenev, J. F. Mariano, M. C. Mateus, J. P. Lourenço, A. Ahmed, M. Hantusch, E. Burkel, and A. M. Botelho do Rego. *Nanomaterials*, **11** (2021):2519. DOI: https://doi.org/10.3390/nano11102519.

[19] O. Ferreira, O. C. Monteiro, A. M. B. do Rego, A. M. Ferraria, M. Batista, R. Santos, S. Monteiro, M. Freire, and E. R. Silva. *J. Environ. Chem. Eng.*, **9** (2021):106735. DOI: https://doi.org/10.1016/j.jece.2021.106735.

[20] T. Fukumura, H. Toyosaki, K. Ueno, M. Nakano, and M. Kawasaki. *New J. Phys.*, **10** (2008):055018. DOI: https://doi.org/10.1088/1367-2630/10/5/055018.

[21] S. R. Joshi, B. Padmanabhan, A. Chanda, I. Mishra, V. K. Malik, N. C. Mishra, D. Kanjilal, and S. Varma. *Appl. Surf. Sci.*, **387** (2016):938–943. DOI: https://doi.org/10.1016/j.apsusc.2016.07.038.

[22] R. Kamble, P. Gaikwad, K. Garadkar, S. Sabale, V. Puri, and S. Mahajan. *J. Iran. Chem. Soc.*, **19** (2022):303–312. DOI: https://doi.org/10.1007/s13738-021-02303-y.

[23] C. Khurana, O. Pandey, and B. Chudasama. *J. Sol-Gel Sci. Technol.*, **75** (2015):424–435. DOI: https://doi.org/10.1007/s10971-015-3715-3.

[24] M. Murakami, Y. Matsumoto, T. Hasegawa, P. Ahmet, K. Nakajima, T. Chikyow, H. Ofuchi, I. Nakai, and H. Koinuma. *J. Appl. Phys.*, **95** (2004):5330–5333. DOI: https://doi.org/10.1063/1.1695598.

[25] A. Sharma, P. Negi, R.J. Konwar, H. Kumar, Y. Verma Shailja, P. C. Sati, B. Rajyaguru, H. Dadhich, N. A. Shah, and P. S. Solanki. *Journal of Materials Science & Technology*, **111** (2022):287–297. DOI: https://doi.org/10.1016/j.jmst.2021.09.014.

[26] W. Geng and K. S. Kim. *Phys. Rev. B*, **68** (2003):125203. DOI: https://doi.org/10.1103/PhysRevB.68.125203.

[27] Z. Zhang, Q. Hou, M. Qi, and S. Sha. *Phys. Scr.*, **97** (2022):045815. DOI: https://doi.org/10.1088/1402-4896/ac5ce0.

[28] V. Blum, R. Gehrke, F. Hanke, P. Havu, V. Havu, X. Ren, K. Reuter, and M. Scheffler. *Comput. Phys. Commun.*, **180** (2009):2175–2196. DOI: https://doi.org/10.1016/j.cpc.2009.06.022.

[29] V. Havu, V. Blum, P. Havu, and M. Scheffler. *J. Comput. Phys.*, **228** (2009):8367–8379. DOI: https://doi.org/10.1016/j.jcp.2009.08.008.

[30] A. Marek, V. Blum, R. Johanni, V. Havu, B. Lang, T. Auckenthaler, A. Heinecke, H. J. Bungartz, and H. Lederer. *J. Phys.: Condens. Matter*, **26** (2014):213201. DOI: https://doi.org/10.1088/0953-8984/26/21/213201.

[31] V. W. z. Yu, F. Corsetti, A. García, W. P. Huhn, M. Jacquelin, W. Jia, B. Lange, L. Lin, J. Lu, W. Mi, A. Seifitokaldani, Á. Vázquez Mayagoitia, C. Yang, H. Yang, and V. Blum. *Comput. Phys. Commun.*, **222** (2018):267–285. DOI: https://doi.org/10.1016/j.cpc.2017.09.007.

[32] H. J. Monkhorst and J. D. Pack. *Phys. Rev. B.*, **13** (1976):5188–5192. DOI: https://doi.org/10.1103/PhysRevB.13.5188.

[33] B. Hammer, L. B. Hansen, and J. K. Nørskov. "". *Phys. Rev. B.*, **59** (1999):7413–7421. DOI: https://doi.org/10.1103/PhysRevB.59.7413.

[34] C. Adamo and V. Barone. *J. Chem. Phys.*, **110** (1999): 6158–6170. DOI: https://doi.org/10.1063/1.478522.

[35] T. Lu and F. Chen. *J. Comput. Chem.*, **33** (2012): 580–592. DOI: https://doi.org/10.1002/jcc.22885.

[36] K. Momma and F. Izumi. *J. Appl. Crystallogr*, **44** (2011):1272–1276. DOI: https://doi.org/10.1107/S0021889811038970.

[37] P. K. Jha, S. K. Gupta, and I. Lukačević. *Solid State Sci*, **22** (2013):8–15. DOI: https://doi.org/10.1016/j.solidstatesciences.2013.05.003.

[38] K. Yang, Y. Dai, B. Huang, and S. Han. *J. Phys. Chem. B.*, **110** (2006):24011–24014. DOI: https://doi.org/10.1021/jp0651135.

[39] N. Govind, K. Lopata, R. Rousseau, A. Andersen, and K. Kowalski. *J. Phys. Chem. Lett.*, **2** (2011):2696–2701. DOI: https://doi.org/10.1021/jz201118r.

[40] M. Ceotto, L. Lo Presti, G. Cappelletti, D. Meroni, F. Spadavecchia, R. Zecca, M. Leoni, P. Scardi, C. L. Bianchi, and S. Ardizzone. *J. Phys. Chem. C.*, **116** (2012):1764–1771. DOI: https://doi.org/10.1021/jp2097636.

[41] R. Behjatmanesh-Ardakani. *Int. J. Hydrogen Energ.*, **48** (2023):35584–35598. DOI: https://doi.org/10.1016/j.ijhydene.2023.05.352.

[42] J. Xi H. He S. Zhao H. Lu Z. Ji J. Zhang, W. Fu. *J. Alloys Compd.*, **575** (2013):40–47. DOI: https://doi.org/10.1016/j.jallcom.2013.04.007.

[43] S. Livraghi, A. M. Czoska, M. C. Paganini, and E. Giamello. *J. Solid State Chem*, **182** (2009):160–164. DOI: https://doi.org/10.1016/j.jssc.2008.10.012.

[44] D. L. Shieh, Y. S. Lin, J. H. Yeh, S. C. Chen, B. C. Lin, and J. L. Lin. *Chem. Commun.*, **48** (2012):2528–2530. DOI: https://doi.org/10.1039/C2CC16960F.

[45] S. A. Chambers, S. H. Cheung, V. Shutthanandan, S. Thevuthasan, M. K. Bowman, and A. G. Joly. *Chem. Phys.*, **339** (2007):27–35. DOI: https://doi.org/10.1016/j.chemphys.2007.04.024.

[46] S. H. Cheung, P. Nachimuthu, A. G. Joly, M. H. Engelhard, M. K. Bowman, and S. A. Chambers. *Surf. Sci.*, **601** (2007):1754–1762. DOI: https://doi.org/10.1016/j.susc.2007.01.051.

[47] N. N. Bao, H. M. Fan, J. Ding, and J. B. Yi. *J. Appl. Phys.*, **109** (2011):07C302. DOI: https://doi.org/10.1063/1.3535427.

[48] P. Basera, S. Saini, E. Arora, A. Singh, and S. Bhattacharya. *AIP Conf. Proc.*, **2115** (2019):030394. DOI: https://doi.org/10.1063/1.5113233.

[49] J. Atanelov, C. Gruber, and P. Mohn. *Computational Materials Science*, **98** (2015):42–50. DOI: https://doi.org/10.1016/j.commatsci.2014.10.041.

[50] [Q. J. Liu and Z. T. Liu. *Mater. Sci. Semicond. Process.*, **41** (2016):257–260. DOI: https://doi.org/10.1016/j.mssp.2015.09.014.

[51] C. Di Valentin, E. Finazzi, G. Pacchioni, A. Selloni, S. Livraghi, M. C. Paganini, and E. Giamello. *Chem. Phys.*, **339** (2007):44–56. DOI: https://doi.org/10.1016/j.chemphys.2007.07.020.

[52] P. Kubelka and F. Munk. *Z. Tech. Phys.*, **12** (1931): 593–601.

[53] S. Landi, I. R. Segundo, E. Freitas, M. Vasilevskiy, J. Carneiro, and C.J. Tavares. *Solid State Commun.*, **341** (2022):114573. DOI: https://doi.org/10.1016/j.ssc.2021.114573.